Informational Analysis of Time Series of Sentinel-1 Vegetation Indices for Discerning Pest-affected Vegetation Sites: the case of *Toumeyella Parvicornis*

Luciano Telesca[1], Nicodemo Abate[2], Michele Lovallo[3], Rosa Lasaponara[1]
[1]*Institute of Methodologies for Environmental Analysis, National Research Council*, Tito, Italy
Email: luciano.telesca@cnr.it; rosa.lasaponara@cn.it
[2]*Institute of Heritage Science, National Research Council*, Tito, Italy
Email: nicodemo.abate@cnr.it
[3]*ARPAB*, Potenza, Italy
Email: michele.lovallo@arpab.it

***Abstract*—In this study, we examine Sentinel 1 (S1) Synthetic Aperture Radar (SAR) time series to detect and assess pest-induced vegetation anomalies. The S1 time series was analysed using multiple SAR-based data as vegetation indices. The analyses were performed on a case study located in Castel Porziano (central Italy), chosen due to its significant impact from Toumeyella Parvicornis (TP) in recent years. The area of Follonica, which is not yet affected by TP, was used as a comparison. Our goal is to identify patterns associated with TP in the statistical features of S1 data. The methodology employed is the well-established Fisher-Shannon analysis, which characterizes the temporal dynamics of complex time series using two informational measures: the Fisher Information Measure (FIM) and the Shannon Entropy Power (SEP). Analysis of the Receiver Operating Characteristic (ROC) curve indicates that these two measures are highly effective in distinguishing between infected and healthy sites.**

Index Terms*—Sentinel-1; statistics; vegetation; pests

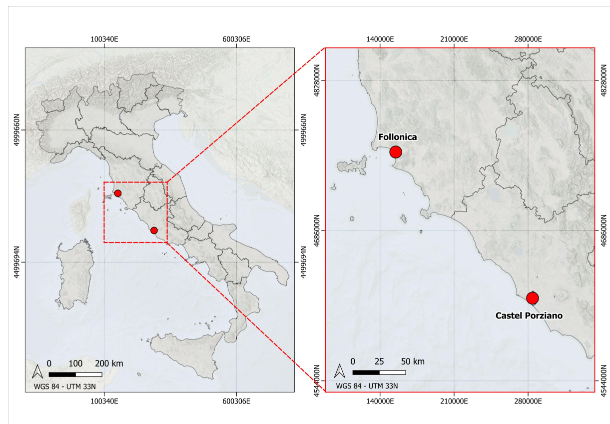

Fig. 1. Study areas.

I. Introduction

Numerous studies have shown that climate change and anthropogenic activities along with the introduction of exotic species, have greatly accelerated the spread of pests into new regions, intensifying their harmful impacts and damage. As a result, forest disturbances caused by parasites have become one of the most pressing global challenges [5].

Detection of affected areas is crucial for mitigation, and satellites offer globally available, systematic datasets, making them ideal for supporting (near) real-time detection of forest disturbances [6]. Satellite Remote Sensing technologies are vital for forest monitoring and identifying vegetation diseases, aiding in the understanding of their spatial and temporal distribution and allowing for the estimation of disturbance rates, severity, and extent [7].

Traditionally, forest cover and change have been monitored using satellite optical data, which have long been used in forest mapping and pest disturbance detection. Recently, various sensors have been tested to assess forest insect disturbances. A comprehensive review by Stahl et al. [8] found that most studies used medium-resolution data (mainly Landsat TM), followed by coarse-resolution data (primarily MODIS), high-resolution data (such as HyMap, QuickBird, RapidEye, and WorldView-2), and very high-resolution data, including LiDAR. The review also highlighted that only one study, by Ortiz et al. [9], combined Synthetic Aperture Radar (SAR) with optical data. Ortiz used TerraSAR-X paired with RapidEye data to detect bark beetle infestations at an early stage. Their results showed that the highest classification accuracy was achieved by combining TerraSAR-X and RapidEye data.

More recent studies have primarily utilized satellite optical data to monitor pest spread, with only a few exploring the potential of SAR. For instance, Huo et al. [10] investigated detection of forest stress caused by European spruce bark beetle infestations, using Sentinel-1 and Sentinel-2 imagery in a test site in southern Sweden. Their findings indicated that the Sentinel-2 red and SWIR bands offered the best separation between healthy and stressed vegetation, while Sentinel-1 and additional Sentinel-2 bands were less effective in Random Forest classification models.

As with other vegetation studies, SAR remains less utilized

 ISBN: 978-1-68558-284-5

compared to optical data, largely due to the greater complexity of processing and interpretation, despite its well-established advantages. SAR can detect changes in vegetation status and moisture content, penetrate the canopy to some extent (depending on frequency), and provide insights into vegetation structure and density. In recent years, several studies have explored the potential of SAR to: (i) monitor deforestation and forest degradation [11], (ii) identify drivers of forest change [12], (iii) detect and categorize fires and fire severity [13], (iv) assess damage from extreme events [14] and drought [15], (v) capture forest seasonality and characterize plant phenology [16], and (vi) classify vegetation, forest types, and forest loss [17].

In this paper, we evaluate the potential of Sentinel-1 SAR time series to detect pest-induced vegetation disturbances caused by Toumeyella parvicornis (TP), an invasive hemipteran species from the Americas. Since its introduction in Italy in 2015, TP has primarily affected *Pinus pinea*. The insect produces large amounts of honeydew, giving infested trees a shiny appearance and promoting the growth of sooty mold, which covers the pine needles and branches. This coating reduces photosynthesis, resulting in tree decline and, in severe cases, death.

The paper is organized as follows. Section II describes the Fisher-Shannon method and the ROC analysis used for the investigation of our series. Section III presents the data and study area. Section IV discusses the results obtained from the analysis, highlighting key findings. Finally, Section V summarizes the conclusions drawn from our study and suggests potential directions for future research.

II. METHODS

To investigate the potential of Sentinel-1 SAR time series in detecting TP-induced vegetation disturbances, we will apply the Fisher-Shannon informational method. To assess the performance of discriminating between infected and uninfected pixels, we will utilize ROC analysis.

A. The Fisher-Shannon method

The informational properties of a time series can be analysed by the Fisher Information Measure (FIM) and the Shannon entropy (SE) that quantify respectively the local and global smoothness of the distribution of a series. The FIM and SE can be utilized for characterizing the complexity of non-stationary time series described in terms of order and organization. The FIM measures the order and organization of the series, and the SE its uncertainty or disorder. The FIM and SE are defined by the following formulae:

$$\text{FIM} = \int_{-\infty}^{\infty} \frac{1}{f(x)} \left(\frac{\partial f(x)}{\partial x} \right)^2 dx \tag{1}$$

$$\text{SE} = -\int_{-\infty}^{\infty} f(x) \log f(x)\, dx \tag{2}$$

where $f(x)$ is the distribution of the series x. Instead of SE, it is generally used the Shannon entropy power (SEP) N_X, defined as positive:

$$N_X = \exp\left(2 \int_{-\infty}^{\infty} f(x) \log f(x)\, dx \right) \tag{3}$$

FIM and N_X are not independent of each other due to the isoperimetric inequality:

$$\text{FIM} \cdot N_X \geq D \tag{4}$$

where D is the dimension of the space (1 for time series). FIM and N_X depend on $f(x)$, whose accurate estimation is crucial to obtain reliable values of informational quantities. For calculating FIM and N_X, we applied the kernel-based approach that is better than the discrete-based approach in estimating the probability density function [18].

Due to the isoperimetric inequality, the Fisher-Shannon Information Plane (FSIP), which has the N_X as the x-axis and FIM as the y-axis, represents a very useful tool to investigate the complexity of time dynamics of signals. For scalar signals, the curve $\text{FIM} \cdot N_X = 1$ separates the FSIP into two parts, and each signal can be represented by a point located only in the space $\text{FIM} \cdot N_X > 1$.

B. The ROC Analysis

Receiver Operating Characteristics (ROC) analysis is utilized to evaluate the performance of classifiers. In binary classification scenarios, instances are classified as either ”positive” or ”negative,” and a classifier assigns these instances to predicted classes. When assessing a classifier with respect to an instance, four potential outcomes can occur. The categorization of the instance is as follows: True Positive (TP) if it is positive and correctly classified as positive, False Negative (FN) if it is positive but incorrectly classified as negative, True Negative (TN) if it is negative and correctly classified as negative, False Positive (FP) if it is negative but erroneously classified as positive [19]. We can define the following ratios, the True Positive rate (TPr) and the False Positive rate (FPr):

$$\text{TPr} = \frac{\text{Number of TP}}{\text{Total positives}} \tag{5}$$

$$\text{FPr} = \frac{\text{Number of FP}}{\text{Total negatives}} \tag{6}$$

A ROC curve is a graphical representation with TPr plotted on the y-axis and FPr on the x-axis, depending on a threshold. In ROC space, the point $(0, 1)$ signifies perfect classification, and one point is considered superior to another if it lies to the northwest of the first point. The diagonal line, represented by the equation $y = x$, corresponds to random classification. Each point on the ROC curve corresponds to a tradeoff between TPr and FPr associated with a threshold. Typically, to optimize this tradeoff, the point on the ROC curve closest to $(0, 1)$ is chosen, and the corresponding threshold is utilized for classification. Also, the Area Under the ROC Curve (AUC) is frequently employed to quantify the classifier’s performance.

 ISBN: 978-1-68558-284-5

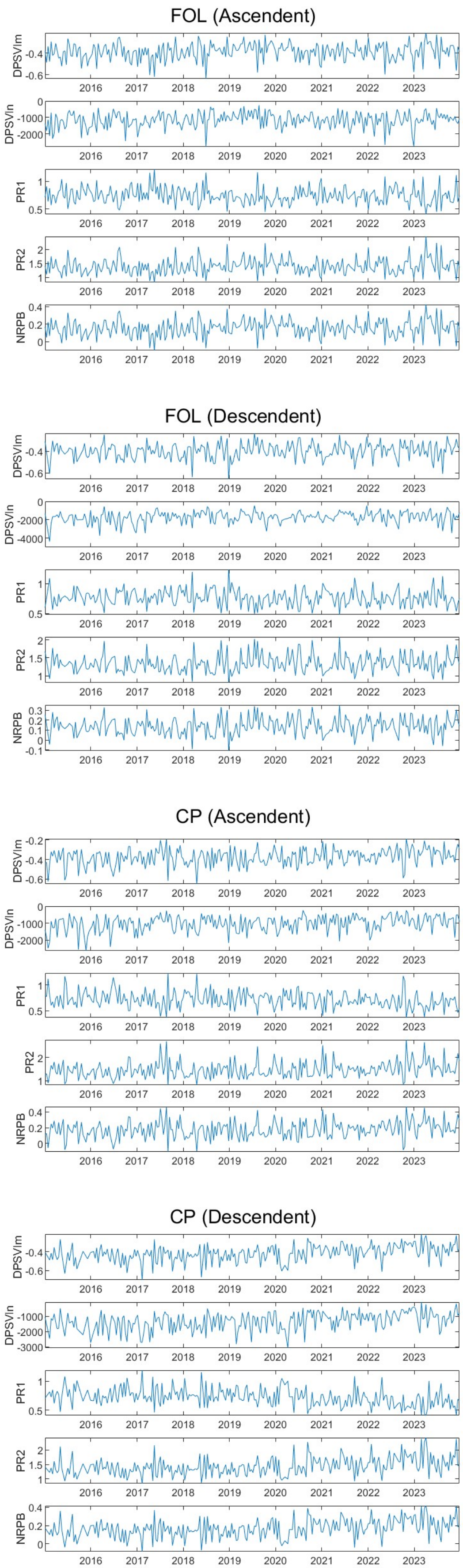

Fig. 2. Example of time series.

III. Data and Study Area

Castel Porziano (CP) is a Presidential Estate near Rome, spanning 6,039 hectares. This historically and environmentally significant site is located in Lazio along the coast. CP was selected as a case study due to the severe impact of TP, which caused widespread desiccation and, in many cases, tree mortality in subsequent years. To evaluate the discrimination capability of SAR data, Follonica (FL) was chosen as a control site. Situated near Castel Porziano, it shares the same *Pinus pinea L.* species but had no documented TP infestation as of 2023 (Figure 1). FL and CP are geographically similar. Both sites are coastal pine forests located along the same coastline, approximately 200 km apart. In addition to having the same dominant vegetation and coastal exposure, they fall within the same Köppen climate classification (Cs—temperate climate with dry summers). This climate type, which characterizes the Tyrrhenian coastal strip from Liguria to Calabria, as well as the southern Adriatic and Ionian coasts of Italy, is a key factor in defining the environmental context of the study [20].

The investigation was based on Sentinel-1 VV and VH time series (2015–2022), accessible through Google Earth Engine (GEE). The sampling interval is 12 days. For the CP, 150 pixels representing the infected areas were selected, while 150 pixels were similarly chosen for the FL site. These 150 points were randomly selected within the pine forest area, as indicated by Corine Land Cover. For both sites, the primary Sentinel-1 bands (VV and VH) from both ascending and descending orbits were downloaded. Then, five SAR-based indices (Table I) were calculated by using the following formulae:

TABLE I. SAR-INDICES.

Name	Index	[Reference]
Polarimetric ration 1	PR1	[1]
Polarimetric ration 2	PR2	[2]
Normalized Ration Procedure between Bands	NRPB	[3]
Dual Pol. SAR Vegetation Index, modified	DPSVIm	[4]
Dual Pol. SAR Vegetation Index, normalized	DPSVIn	[4]

$$\text{PR1} = \frac{VV}{VH} \tag{7}$$

$$\text{PR2} = \frac{VH}{VV} \tag{8}$$

$$\text{NRPB} = \frac{VH\text{-}VV}{VH\text{+}VV} \tag{9}$$

$$\text{DPSVIm} = \frac{\max(VV) - (VV + VH)}{1.414213562373095 \times \left(\frac{(VV+VH)}{VV}\right) \times VH} \tag{10}$$

$$\text{DPSVIn} = VH \times \left(\frac{VV^2 + (VV + VH)}{1.414213562373095}\right) \tag{11}$$

Cross-polarization ratio indices (i.e., PR1 and PR2) are highly sensitive to variations in vegetation structure and moisture content, allowing them to effectively capture subtle temporal dynamics. This sensitivity renders them particularly valuable for detecting seasonal changes and vegetation stress. In contrast, NRPB quantifies differences in scattering mechanisms between the VV and VH channels. It is especially responsive in regions characterized by sparse vegetation or lower canopy density, where soil moisture and surface scattering predominate. The Dual-Polarized SAR Vegetation Index (Normalized) (DPSVIn) exhibits a high sensitivity to volume scattering effects that are characteristic of dense vegetation and canopy structures, while effectively mitigating the influence of absolute backscatter variations. This dual functionality renders DPSVIn particularly well-suited for comparative analyses of vegetation structure across diverse environmental settings and sensor configurations. Similarly, the modified DPSVIm represents a further refinement of the DPSVIn, integrating advanced corrections to enhance vegetation discrimination, particularly under challenging environmental conditions.

IV. Results

We analyzed 150 pixel time series from CP and FOL sites, spanning from 2015 to 2023 with a 12-day sampling interval. Both ascendent and descendent orbits were considered, and for each pixel, we calculated the five vegetation indices defined in Section III. Figure 2 presents these indices as examples for two pixels in the CP and FOL sites across both orbit types.

Subsequently, we applied FS analysis to compute the FIM and N_X for each vegetation index across all 150 pixels in both sites. Figure 3 displays the boxplots of N_X and FIM for the five vegetation indices in ascendent and descendent orbits. On average, TP-infected sites exhibit a higher N_X and lower FIM than healthy sites in descendent orbits for most indices. Conversely, in ascendent orbits, the trend is generally reversed, except for DPSVIn.

To quantitatively evaluate the discrimination performance of the five vegetation indices between infected and uninfected sites, we applied ROC analysis. The results are shown in Tables II, III, IV, and V.

Considering N_X for the descendent orbit, PR1 and DPSVIn demonstrate good performance, with AUC values of 0.75 and 0.79, and TPRs of 71% and 68%, respectively. For N_X in the descendent orbit, all indices except DPSVIn show optimal performance, with large AUC (from 0.82 to 0.90) and TPR (from 73% to 82%) values and low FPR (from 12% to 21%).

For FIM in the ascendent orbit, PR1 and DPSVIn also show good performance, similar to N_X in the ascendent orbit. AUC values range from 0.70 to 0.79, with TPRs around 65%-71%.

In the descendent orbit, all indices except DPSVIn exhibit optimal discrimination performance for FIM, with AUC values ranging from 0.81 to 0.89, TPRs varying between 70% and 79%, and FPRs between 9% and 23%.

The observed difference in Fisher-Shannon response between infected and uninfected trees may be associated with variations in the photosynthetic activity. The *Pinus pinea* canopy in healthy conditions exhibits a well-defined seasonal pattern, which is effectively captured by SAR signal, reflecting order and organization within the time series. In contrast, TP infestation reduces photosynthetic activity, leading to widespread tree desiccation and a loss of phenological cycles. This results in a diminished seasonality and increased disorder in the SAR signal. The two adopted metrics effectively highlight both healthy and unhealthy vegetation conditions. Therefore, the classification of FIM and SE metrics within the SAR time series enhances the ability to discriminate alterations in vegetation structure and moisture content induced by insect infestations or diseases

V. Conclusion and future works

This study investigates the potential of using Sentinel-1 (S1) data to monitor and detect forest vegetation infestations and insect-related diseases, with a focus on two test sites in Italy: Castel Porziano, which is affected by *Toumeyella parvicornis*, and Follonica, which remains unaffected. The primary difference in vegetation health between the two sites is the presence of the parasite. The findings reveal a significant influence of the parasite on the S1 SAR signal, which correlates directly with vegetation changes caused by: (i) canopy drying and reduced humidity, and (ii) a gradual decline in canopy density due to the suppression of new needle growth. This effect is clearly visible through the statistical methods employed in this study. The application of ROC analysis to the Fisher-Shannon-based metrics allowed for the evaluation of the performance of S1 vegetation indices across two orbit types (Ascending and Descending). The highest discrimination performance was observed with N_X of PR2 and with FIM of NRPB both in the descending orbit. Our results clearly show that S1 data can effectively detect changes in vegetation structure and moisture content linked to insect infestations or diseases, improving the identification of backscattering signal alterations and recognizing deviations from typical patterns. This capability facilitates a clear distinction between healthy and unhealthy areas. Descending acquisitions generally yield superior results compared to ascending acquisitions when monitoring vegetation with SAR. This advantage is primarily attributable to differences in illumination geometry, shadowing, as well as moisture content and dielectric properties. In descending mode, SAR satellites typically acquire images in the afternoon when the sun is at a higher angle. This configuration minimizes terrain shadowing and promotes a more consistent backscatter response from vegetation. Conversely, ascending acquisitions, usually obtained in the early morning, are more prone to pronounced shadow effects due to lower sun angles, which can diminish the visibility of certain features. Furthermore, vegetation generally exhibits higher moisture content during early morning hours (when ascending passes occur) due to dew formation and overnight cooling. The increased moisture enhances signal absorption and reduces backscatter, complicating the discrimination of vegetation structures. During descending passes, vegetation tends to dry slightly due to daytime heating, resulting in a more stable and consistent radar response. Both illumination geometry and moisture content contribute to a more stable and

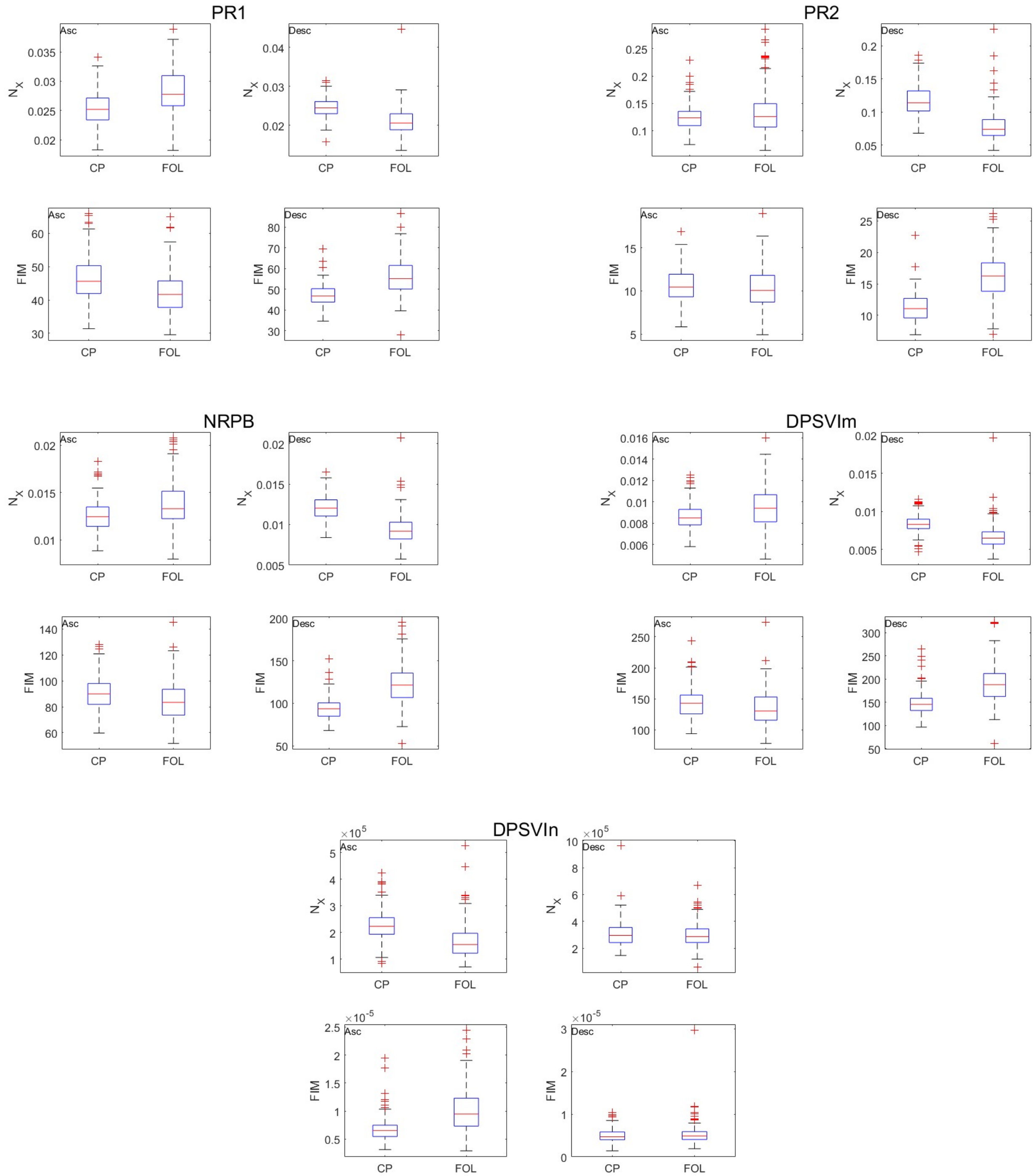

Fig. 3. Boxplots of N_X and FIM of the five vegetation indices for the ascendent and descendent orbits.

 ISBN: 978-1-68558-284-5

TABLE II. RESULTS OF THE ROC ANALYSIS FOR N_X FOR THE ASCENDENT TYPE OF ORBIT. (THE * REFERS TO THE VALUE OF TPR AND FPR CORRESPONDING TO THE OPTIMAL THRESHOLD)

	PR1	PR2	NRPB	DPSVIm	DPSVIn
AUC	0.75	0.55	0.66	0.65	0.79
Optimal threshold	$2.6 \cdot 10^{-2}$	$1.3 \cdot 10^{-1}$	$1.3 \cdot 10^{-2}$	$9 \cdot 10^{-3}$	$1.8 \cdot 10^{5}$
TPr*	0.71	0.45	0.54	0.59	0.68
FPr*	0.34	0.33	0.31	0.31	0.15

TABLE III. RESULTS OF THE ROC ANALYSIS FOR N_X FOR THE DESCENDENT TYPE OF ORBIT. (THE * REFERS TO THE VALUE OF TPR AND FPR CORRESPONDING TO THE OPTIMAL THRESHOLD)

	PR1	PR2	NRPB	DPSVIm	DPSVIn
AUC	0.82	0.90	0.89	0.84	0.53
Optimal threshold	$2.3 \cdot 10^{-2}$	$9.3 \cdot 10^{-2}$	$1.1 \cdot 10^{-2}$	$7.5 \cdot 10^{-3}$	$3.2 \cdot 10^{5}$
TPr*	0.73	0.8	0.82	0.81	0.66
FPr*	0.21	0.12	0.13	0.21	0.54

TABLE IV. RESULTS OF THE ROC ANALYSIS FOR FIM FOR THE ASCENDENT TYPE OF ORBIT. (THE * REFERS TO THE VALUE OF TPR AND FPR CORRESPONDING TO THE OPTIMAL THRESHOLD)

	PR1	PR2	NRPB	DPSVIm	DPSVIn
AUC	0.70	0.56	0.64	0.6	0.79
Optimal threshold	43.34	10.25	82.86	136.4	$7.8 \cdot 10^{-6}$
TPr*	0.65	0.54	0.5	0.59	0.71
FPr*	0.34	0.43	0.29	0.39	0.19

TABLE V. RESULTS OF THE ROC ANALYSIS FOR FIM FOR THE DESCENDENT TYPE OF ORBIT. (THE * REFERS TO THE VALUE OF TPR AND FPR CORRESPONDING TO THE OPTIMAL THRESHOLD)

	PR1	PR2	NRPB	DPSVIm	DPSVIn
AUC	0.81	0.87	0.89	0.83	0.51
Optimal threshold	50.91	14.07	104.35	159.75	$4.8 \cdot 10^{-6}$
TPr*	0.7	0.75	0.79	0.78	0.53
FPr*	0.19	0.09	0.17	0.23	0.47

interpretable radar response during descending passes. Nevertheless, the optimal acquisition mode depends on specific environmental conditions, sensor characteristics, and research objectives. Further investigations will be carried out to explore in greater depth the potential and limitations of Sentinel-1 data. Nevertheless, the value of these preliminary findings lies in demonstrating that early detection of infestations is crucial for developing mitigation strategies and effectively preventing their rapid spread.

ACKNOWLEDGMENT

This study was supported by the project ”Coelum Spies of Climate change and tools for mitigating the effects: EO and AI based methodological approach for Urban Park Management”, funded by the National Research Council of Italy.

REFERENCES

[1] P.-L. Frison, et al., ”Potential of Sentinel-1 Data for Monitoring Temperate Mixed Forest Phenology,” Remote Sensing, vol. 10, pp. 2049, 2018. doi:10.3390/rs10122049

[2] J. Alvarez-Mozos, J. Villanueva, M. Arias, and M. Gonzalez-Audicana, ”Correlation Between NDVI and Sentinel-1 Derived Features for Maize,” in 2021 IEEE International Geoscience and Remote Sensing Symposium IGARSS, Brussels, Belgium, pp. 6773–6776, 2021. doi:10.1109/IGARSS47720.2021.9554099

[3] J. N. Hird, E. R. DeLancey, G. J. McDermid, and J. Kariyeva, ”Google Earth Engine, Open-Access Satellite Data, and Machine Learning in Support of Large-Area Probabilistic Wetland Mapping,” Remote Sensing, vol. 9, pp. 12, 2017. doi:10.3390/rs9121315

[4] S. Periasamy, ”Significance of Dual Polarimetric Synthetic Aperture Radar in Biomass Retrieval: An Attempt on Sentinel-1,” Remote Sensing of Environment, vol. 217, pp. 537–549, 2018. doi:10.1016/j.rse.2018.09.003

[5] F. Niccoli, J. P. Kabala, S. Altieri, S. Faugno, and G. Battipaglia, ”Impact of *Toumeyella parvicornis* Outbreak in *Pinus pinea* L. Forest of Southern Italy: First Detection Using a Dendrochronological, Isotopic and Remote Sensing Analysis,” Forest Ecology and Management, vol. 566, pp. 122086, 2024. doi:10.1016/j.foreco.2024.122086

[6] J. Verbesselt, A. Zeileis, and M. Herold, ”Near Real-Time Disturbance Detection Using Satellite Image Time Series,” Remote Sensing of Environment, vol. 123, pp. 98–108, 2012. doi:10.1016/j.rse.2012.02.022

[7] C. Senf, R. Seidl, and P. Hostert, ”Remote Sensing of Forest Insect Disturbances: Current State and Future Directions,” International Journal of Applied Earth Observation and Geoinformation, vol. 60, pp. 49–60, 2017. doi:10.1016/j.jag.2017.04.004

[8] A. T. Stahl, R. Andrus, J. A. Hicke, A. T. Hudak, B. C. Bright, and A. J. H. Meddens, ”Automated Attribution of Forest Disturbance Types from Remote Sensing Data: A Synthesis,” Remote Sensing of Environment, vol. 285, pp. 113416, 2023. doi:10.1016/j.rse.2022.113416

[9] S. M. Ortiz, J. Breidenbach, and G. Kändler, ”Early Detection of Bark Beetle Green Attack Using *TerraSAR-X* and *RapidEye* Data,” Remote Sensing, vol. 5, pp. 1912–1931, 2013. doi:10.3390/rs5041912

[10] L. Huo, H. J. Persson, and E. Lindberg, ”Early Detection of Forest Stress from *European* Spruce Bark Beetle Attack, and a New Vegetation Index: Normalized Distance Red & *SWIR* (NDRS),” Remote Sensing of Environment, vol. 255, pp. 112240, 2021. doi:10.1016/j.rse.2020.112240

[11] X. Tang, K. H. Bratley, K. Cho, E. L. Bullock, P. Olofsson, and C. E. Woodcock, ”Near Real-Time Monitoring of Tropical Forest Disturbance by Fusion of *Landsat*, *Sentinel*-2, and *Sentinel*-1 Data,” Remote Sensing of Environment, vol. 294, pp. 113626, 2023. doi:10.1016/j.rse.2023.113626

[12] B. Slagter et al., ”Monitoring Direct Drivers of Small-Scale Tropical Forest Disturbance in Near Real-Time with *Sentinel*-1 and *Sentinel*-

2 Data," Remote Sensing of Environment, vol. 295, pp. 113655, 2023. doi:10.1016/j.rse.2023.113655

[13] R. Lasaponara, C. Fattore, and G. Modica, "Imaging Burned Areas and Fire Severity in *Mediterranean* Fragmented Ecosystems Using Sentinel-1 and Sentinel-2: The Case Study of Tortolì–Ogliastra Fire (Sardinia)," IEEE Geoscience and Remote Sensing Letters, vol. 20, pp. 1–5, 2023. doi:10.1109/LGRS.2023.3324945

[14] M. Dalponte, Y. T. Solano-Correa, D. Marinelli, S. Liu, N. Yokoya, and D. Gianelle, "Detection of Forest Windthrows with Bitemporal *COSMO-SkyMed* and *Sentinel*-1 *SAR* Data," *Remote Sensing of Environment*, vol. 297, pp. 113787, 2023. doi:10.1016/j.rse.2023.113787

[15] K. Schellenberg et al., "Potential of Sentinel-1 SAR to Assess Damage in Drought-Affected Temperate Deciduous Broadleaf Forests," Remote Sensing, vol. 15, pp. 1004, 2023. doi:10.3390/rs15041004

[16] K. Soudani et al., "Potential of C-Band Synthetic Aperture Radar Sentinel-1 Time-Series for the Monitoring of Phenological Cycles in a Deciduous Forest," International Journal of Applied Earth Observation and Geoinformation, vol. 104, pp. 102505, 2021. doi:10.1016/j.jag.2021.102505

[17] M. Lechner, A. Dostálová, M. Hollaus, C. Atzberger, and M. Immitzer, "Combination of Sentinel-1 and Sentinel-2 Data for Tree Species Classification in a Central European Biosphere Reserve," Remote Sensing, vol. 14, pp. 2687, 2022. doi:10.3390/rs14112687

[18] L. Telesca and M. Lovallo, "On the Performance of Fisher Information Measure and Shannon Entropy Estimators," Physica A: Statistical Mechanics and Its Applications, vol. 484, pp. 569–576, 2017.

[19] T. Fawcett, "An Introduction to ROC Analysis," Pattern Recognition Letters, vol. 27, pp. 861–874, 2006.

[20] H. E. Beck, N. E. Zimmermann, T. R. McVicar, N. Vergopolan, A. Berg, and E. F. Wood, "Present and Future Köppen-Geiger Climate Classification Maps at 1-km Resolution," Scientific Data, vol. 5, pp. 180214, 2018.